Electron Tunneling in Organic Bilayer Light-Emitting Diodes with a Novel Electron-Transporting Polymer

J. Pommerehne, A. Selz, K. Book, F. Koch, U. Zimmermann, Chr. Unterlechner, J. H. Wendorff, W. Heitz, and H. Bässler*

Institute of Physical and Macromolecular Chemistry and Center of Material Science, Philipps-University, Hans-Meerwein-Strasse, D-35032 Marburg, Germany

Received June 23, 1997; Revised Manuscript Received October 15, 1997[⊗]

ABSTRACT: Bilayer light-emitting diodes have been fabricated by combining hole-transporting tristilbeneamine or poly[(2,5-bis((2-ethylhexyl)oxy)-1,4-phenylene)vinylene] (EH-PPV) with new electron-transporting polystyrene copolymer carrying *tert*-butyl or CF_3-substituted quaterphenyl substituents as charge-transporting moieties. The latter are resistent against recrystallization and favor internal charge accumulation by virtue of low-lying HOMO and LUMO positions. When LEDs with interfacial electron barriers ≥0.5 eV are addressed by a rectangular voltage pulse, a step-function-like onset of the electroluminescence is observed after an extended delay time that depends on the time period between successive voltage pulses. It reflects the commencement of electron tunneling once the interfacial charge density has reached a critical value. The experimental results are in accordance with model calculations.

1. Introduction

Electroluminescence from organic light-emitting diodes is the result of the recombination of electrons and holes injected from the contacts and the concomitant formation of a fluorescent state. The bimolecular character of the reaction implies that its rate scales with the product of the electron and hole densities established inside the diode.[1] Accordingly, strategies to increase the emission intensities include the improvement of injection,[2,3] notably of minority carrier injection, and the insertion of internal energy barriers that give rise to space charge accumulation.[4−7] The latter is realized in bilayer LEDs that combine a hole-transporting material with low oxidation potential with an electron-transporting material whose HOMO (highest molecular orbital) and LUMO (lowest unoccupied orbital) positions are sufficiently below those of the former. A low-lying LUMO of the cathodic layer will simultaneously favor electron injection. On the other hand, efficient electroluminescence requires the formation of a singlet state of one of the constituent molecules and, concomitantly, the passage of one sort of carrier across the internal barrier. It is intuitively obvious, therefore, that the operation of a bilayer (or multilayer) LED[8,9] will depend in a complicated way on the energy barriers existing at the electrodes and the internal interface(s).

While there is a large selection of hole-transporting materials, only few electron transporters have been used so far. These include (8-hydroxyquinoline)aluminum (Alq_3),[10] triazoles,[11] and notably, various derivatives of oxadiazole.[7,12−15] Various low molecular weight compounds have the disadvantage of a tendency to crystallize. This is prohibitive for LED fabrication because grain boundaries may act as sources for leakage currents. One of the purposes of this paper is to report on the synthesis and successful use of a new type of electron-transporting material. It consists of a statistical copolymer of polystyrene with a substituted vinyl-quaterphenyl chain. The polymers are resistent to crystallization and have a low reduction potential, notably if the substituents are CF_3 groups. This facilitates electron injection. Since high internal energy barriers are established if combined with usual hole-transporting materials, one can also study their effect on the performance of bilayer LEDs. The key result will be that in this case it is electron tunneling across the internal energy barrier that is rate controlling for both carrier injection and light emission. It leads to a step-like onset of electroluminescence upon addressing the LED by a rectangular voltage pulse.

2. Experimental Section

2.1. Materials. 3-Bromotoluene (Aldrich), boronic acid trimethyl ester (Fluka), 4-bromobiphenyl (Avokado), and 3,5-bis(trifluoromethyl)bromobenzene (Avokado) were used as received. 4-Bromo-4′-iodobiphenyl was prepared according to Wirth.[16] The synthesis of (3-methylphenyl)boronic acid is described in ref 17. Tristilbeneamine was synthesized as described.[18] Polycarbonate was received from Bayer; polysulfone, from BASF.

3-Methyl-4″-bromo-1,1′:4′,1″-terphenyl. (3-Methylphenyl)boronic acid (35.0 g, 0.257 mol), 4-bromo-4′-iodobiphenyl (92.26 g, 0.257 mol), and tetrakis(triphenylphosphino)palladium(0) (5.04 g, 4.37 mmol) are suspended in a degassed mixture of toluene (400 mL) and 2 M Na_2CO_3 (400 mL). The two-phase mixture was stirred for 3 days at 100 °C. The organic phase was washed three times with 5% HCl (100 mL) and dried with $MgSO_4$. After the solvent was evaporated, the product was recrystallized from acetone. Yield: 57.89 g (70% theoretical). Mp: 162−163 °C. ^{1}H-NMR (300 MHz, $CDCl_3$): δ/ppm = 2.39 (s, 3H, $-CH_3$), 7.13−7.64 (m, 12 H, aromatic protons). ^{13}C-NMR (75 MHz, $CDCl_3$): δ/ppm = 21.65, 121.68, 124.26, 127.23, 127.74, 127.94, 128.33, 128.71, 128.86, 132.02, 138.55, 138.87, 139.78, 140.63, 140.79. IR (KBr), ν/cm^{-1}: 2976 (w), 1604 (s), 1475 (m), 1386 (m), 1078 (m), 998 (w), 817 (s), 779 (s), 693 (s). MS (EI, *m/e*): 324/93.84%, 323/22.36% (M^+), 322/100%. Anal. Calcd for $C_{19}H_{15}Br$ (323.23): C, 70.60; H, 4.68; Br, 24.72. Found: C, 70.61; H, 4.59; Br, 24.61.

3-Methyl-3‴,5‴-bis(trifluoromethyl)-1,1′:4′,1″:4″,1‴-quaterphenyl. 3-Methyl-4″-(dihydroxyboranyl)-1,1′:4′,1″-terphenyl (30.0 g, 0.104 mol), 3,5-bis(trifluoromethyl)bromobenzene (29.3 g, 0.1 mol), and tetrakis(triphenylphosphino)palladium(0) (2.54 g, 2.2 mmol) were added to a degassed mixture of toluene (350 mL) and 2 M Na_2CO_3 solution (350 mL). After 3 days at 100 °C the reaction mixture was washed three times with 5% HCl and dried with $MgSO_4$. After the solvent was removed, a white, crystalline solid was obtained. Yield: 28.5 g (56% theoretical). Mp 145−147 °C. ^{1}H-NMR (300 MHz, $CDCl_3$): δ/ppm = 2.41 (s, 3H, $-CH_3$), 7.17−8.03 (m, 15H, aromatic protons). ^{13}C-NMR (75 MHz, $CDCl_3$): δ/ppm = 21.40, 120.78, 121.34, 124.03, 126.91, 127.24,

[⊗] Abstract published in *Advance ACS Abstracts,* December 1, 1997.

S0024-9297(97)00905-4 CCC: $14.00

Table 1. Copolymerization of Ia (No a) and Ib (No b−f) (0.5 g) with Styrene at 60 °C in Toluene (25 mL) for 1 Day

no.	amt of styrene/g	[AIBN][a] (mol %)	yield (% th)	I[b] (mol %)	*m*[c] (mol %)	*m*[c] (wt %)	T_g	M_w[e]
a[f]	16.6	1	50	6.6	14.3	41.6	155	42 000
b	19	1.5	51	1.2	1.4	6.0	123	36 600
c[d]	4.5	3.0	49	2.4	2.5	10.4	124	20 300
d	2.83	1.5	36	3.8	3.6	14.4	132	31 400
e	2.0	1.5	38	5.3	3.7	14.8	136	31 400
f[f]	1.5	1.5	22	6.9	3.9	15.5	139	23 900

[a] Based on styrene. [b] Ia,b in the monomer mixture. [c] Ia,b in the polymer calculated from ^{1}H-NMR and UV. [d] Reaction time 2 days. [e] By GPC using universal calibration. [f] Used in LEC devices.

127.51, 127.53, 127.68, 127.70, 128.12, 128.63, 132.08, 136.88, 138.32, 138.68, 140.38, 140.73, 141.22, 142.71. IR (KBr), ν/cm^{-1}: 2952 (s), 2866, 1460 (s), 1385 (s), 1277 (s), 1211 (w), 1180 (w), 1123 (w), 1061 (s), 1008 (w), 899 (w), 824 (s), 787 (s), 700 (m). MS (EI, *m/e*): 457/100.0% (M^+), 234/16.21%. Anal. Calcd for $C_{27}H_{18}F_6$ (456.43): C, 71.05; H, 3.97. Found: C, 70.63; H, 3.90%.

3-Methyl-3‴,5‴-di-*tert*-butyl-1,1′:4′,1″:4″,1‴-quaterphenyl. In a procedure analogous to that given above 3,5-di-*tert*-butylbromobenzene (26.9 g, 0.1 mol) was reacted. The amounts of the other compounds were not changed. Yield: 30.4 g (70% theoretical). Mp: 164−165 °C. ^{1}H-NMR (300 MHz, $CDCl_3$): δ/ppm = 1.42 (s, 18H, 2-C$(CH_3)_3$), 2.49 (s, 3H, −CH_3), 7.21−7.78 (m, 15H, aromatic protons). ^{13}C-NMR (75 MHz, $CDCl_3$): δ/ppm = 21.51, 31.50, 34.96, 121.48, 121.56, 124.11, 127.21, 127.27, 127.50, 127.80, 128.04, 128.67, 138.34, 139.30, 139.61, 140.13, 140.20, 140.68, 141.32, 141.48, 151.15. IR (KBr), ν/cm^{-1}: 2952 (s), 2855 (w), 1595 (s), 1503 (m), 1479 (s), 1436 (s), 1390 (s), 1361 (s), 1246 (s), 1201 (w), 1119 (w), 899 (w), 877 (m), 856 (w), 823 (s), 784 (s), 711 (m), 694 (m). MS (EI, *m/e*): 433/26.78%, 432/78.93% (M^+), 277/77.30%, 244/100.00%, 77/20.03%, 57/72.18%. Anal. Calcd for $C_{33}H_{36}$ (432.65): C, 91.61; H, 8.39. Found: C, 90.01; H, 8.33.

3-(Benzyltriphenylphosphonium bromide)-3‴,5‴-bis(trifluoromethyl)-1,1′:4′,1″:4″,1‴-quaterphenyl. 3-Methyl-3‴,5‴-bis(trifluoromethyl)-1,1′:4′,1″:4″,1‴-quaterphenyl (38.6 g, 50 mmol) was heated to reflux in CCl_4 (200 mL). Bromine (2.6 mL, 50 mmol) dissolved in CCl_4 (20 mL) was added under irradiation with a 500 W UV lamp within 1 h at in such a rate that the refluxing solvent was nearly colorless. Reflux was continued for 2 h. The reaction mixture was treated with $NaHSO_3$ solution and $MgSO_4$, and the solvent evaporated. The residue was dissolved in $CHCl_3$ (200 mL), triphenylphosphine (13.1 g, 50 mmol) was added, and the mixture was heated to reflux for 18 h. The reaction was poured into diethyl ether (1.5 L). The phosphonium salt was filtered off and washed with diethyl ether (300 mL). Yield: 22 g (56% theoretical). ^{1}H-NMR (300 MHz, $CDCl_3$): δ/ppm = 5.49 (d, 2H, J = 14 Hz, PCH_2), 7.10−7.23 (m, 830H). ^{13}C-NMR (75 MHz, $CDCl_3$): δ/ppm = 31.15, 117.37, 118.50, 126.64, 126.96, 127.33, 127.58, 127.71, 127.92, 128.04, 129.29, 130.02, 130.18, 130.62, 132.17, 134.47, 134.60, 134.90, 137.01, 138.99, 139.16, 140.52, 141.04, 142.75. IR (KBr), ν/cm^{-1}: 3055 (s), 2854 (m), 1605 (s), 1482 (s), 1436 (s), 1380 (s), 1284 (s), 1179 (s), 997 (m), 894 (s), 825 (s), 800 (s), 746 (s), 686 (s), 615 (w), 547 (w). Anal. Calcd for $C_{45}H_{32}BrF_6P$ (796.13): C, 67.83; H, 4.05. Found: C, 67.53; H, 3.96.

3-(Benyzltriphenylphosphonium bromide)-3‴,5‴-di-*tert*-butyl-1,1′:4′,1″:4″,1‴-quaterphenyl. 3-Methyl-3‴,5‴-di-*tert*-butyl-1,1′; 4′,1′; 4″,1‴-quaterphenyl (21.6 g, 50 mmol) were converted to the phosphonium salt using the procedure given above. Yield: 18.8 g (44% theoretical). ^{1}H-NMR (300 MHz, $CDCl_3$): δ/ppm = 1.34 (s, 18H, 2-C$(CH_3)_2$), 5.46 (d, 2H, J = 14 Hz, PCH_2, P−^{1}H coupling), 7.26−7.74 (m, 30H). ^{13}C-NMR (75 MHz, $CDCl_3$): δ/ppm = 31.56, 35.01, 117.42, 118.56, 121.59, 127.22, 127.33, 127.88, 130.10, 130.26, 134.47, 134.60, 134.98, 138.64, 139.04, 139.98, 140.11, 151.23. Anal. Calcd for $C_{51}H_{50}BrP$ (772.28): C, 79.25; H, 6.52; Br, 10.22; P, 4.01. Found: C, 78.12; H, 6.38, Br, −P, −.

3-Vinyl-3‴,5‴-bis(trifluoromethyl)-1,1′:4′,1″:4″,1‴-quaterphenyl (Ib). The phosphonium salt (23.9 g, 30 mmol) was suspended in a 37% solution of formaldehyde (171 mL). NaOH (12 N) (25.8 mL) was added over 1 h; the white suspension was stirred for an additional 4 h, and extracted 5 times with toluene (50 mL each). The organic phase was dried using $MgSO_4$, followed by flash chromatography with acidic Al_2O_3 (100 g). The product was obtained as a white, crystalline material after removing the solvent and recrystallization from methanol. Yield: 11.36 g (80% theoretical). Mp: 135.5 °C. UV (THF, 25 °C, λ_{max}): 303 nm (ϵ = 43 998 L mol^{-1} cm^{-1}). ^{1}H-NMR (300 MHz, $CDCl_3$): δ/ppm = 5.34 (dd, 1H), 5.85 (dd, 1H), 6.84 (dd, 1H), 7.26−8.08 (m, 15H). ^{13}C-NMR (75 MHz, $CDCl_3$): δ/ppm = 114.41, 121.02, 121.67, 125.16, 125.37, 126.64, 127.13, 127.53, 127.75, 127.77, 127.91, 129.13, 132.30, 136.86, 137.17, 138.27, 139.12, 140.68, 140,94, 141.36, 142.91. IR (KBr), ν/cm^{-1}: 2960 (m), 1598 (w), 1465 (w), 1283 (s), 1276 (s), 1203 (s), 1181 (s), 1128 (s), 1063 (m). 993 (w), 929 (w), 898 (m), 825 (s), 800 (s), 703 (m), 682 (m). MS (EI, *m/e*): 468/100% (M^+), 234/16.51%. Anal. Calcd for $C_{28}H_{18}F_6$ (468.44): C, 71.79; H, 3.87; F, 24.33. Found: C, 72.27; H, 4.37; F, −.

3-Vinyl-3‴,5‴-di-*tert*-butyl-1,1′:4′,1″:4″,1‴-quaterphenyl (Ia). The phosphonium salt (23.2 g, 30 mmol) was reacted as given above. Yield: 9.86 g (74% theoretical). Mp: 154 °C. UV (THF, 25 °C, λ_{max}): 300 nm (ϵ = 44 256 L mol^{-1} cm^{-1}). ^{1}H-NMR (300 MHz, $CDCl_3$) δ/ppm = 1.39 (s, 18H, 2-C$(CH_3)_3$), 5.30 (dd, 1H), 5.83 (dd, 1H), 6.80 (dd, 1H), 7.17−7.71 (m, 15H). ^{13}C-NMR (75 MHz, $CDCl_3$): δ/ppm = 31.47, 34.92, 114.17, 121.46, 121.53, 124.99, 125.06, 126.48, 127.19, 127.30, 127.49, 127.79, 128.92, 136.75, 138.04, 139.19, 139.79, 139.91, 140.08, 140.97, 141.50, 151.12. IR(KBr), ν/cm^{-1}: 2960 (m), 1595 (m), 1478 (w), 1389 (w), 1361 (m), 1246 (m), 989 (w). 900 (w), 878 (w), 824 (s), 795 (s), 711 (m), 554 (w). MS (EI, *m/e*): 444/100% (M^+), 429/26.16%, 57/59.17%. Anal. Calcd for $C_{34}H_{36}$ (444.66): C, 91.84; H, 8.16. Found: C, 91.72; H, 7.83.

Radical Copolymerization with Styrene. The vinyloligophenylene, stryrene, AIBN, and toluene were poured under nitrogen in a Schlenk tube and repeatedly degassed in a freeze/thaw cycle. The polymerization was carried out at 60 °C for 1 day. The polymer was precipitated with methanol (500 mL). Precipitation was twice repeated with toluene/methanol. Amounts and yields are given in Table 1.

^{1}H-NMR (300 MHz, $CDCl_3$): δ/ppm = 1.38 (m, −CH_2− methylene protons), 1.80 (m, −CH− methine protons), 6.52 (m, polystyrene protons), 7.07 (m, polystyrene protons), 7.65−8.02 (m, polyquaterphenyl protons). IR (KBr), ν/cm^{-1}: 3059 (w), 3026 (m), 2921 (m), 2849 (w), 1941 (w), 1870 (w), 1802 (w), 1601 (m), 1493 (m), 1382 (m), 1278 (s), 1261 (m), 1182 (m), 1136 (s), 1062 (w), 1028 (w), 823 (w), 795 (w), 757 (w), 698 (s), 682 (w), 540 (w).

2.2. Device Characterization. Three types of bilayer LEDs were investigated: (i) A combination of a 20% blend of tristilbeneamine (TSA) with polysulfone (PSu) and CF_3-PQP using either calcium, magnesium, or aluminum as cathode materials, (ii) a 20% TSA−PSu blend in contact with *tert*-butyl-PQP using Ca or Mg as cathodes, and (iii) a 20% blend of EH-PPV with polycarbonate (PC) in combination with either CF_3-PQP or *tert*-butyl-PQP (formulas in Chart 1). The hole-transporting layers were spin cast on the top of ITO (Balzers) from a chloroform solution while PQP was spin cast from cyclohexane, which is a nonsolvent for the bottom layer. Both layers were typically between 85 and 100 nm thick. The active area was 0.12 cm^2. Electron injection into CF_3-PQP and *tert*-butyl-PQP was studied with single-layer diodes carrying Ca electrodes.

Current−voltage characteristics were measured by employing a Keithley source measure unit. To record transient electroluminescence (EL), the device was addressed by single

Chart 1. Structure Formulas on the Hole- (TSA, EH-PPV) and Electron-Transporting (R-PQP) Materials

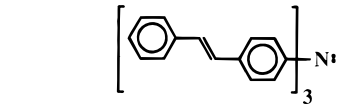

TSA

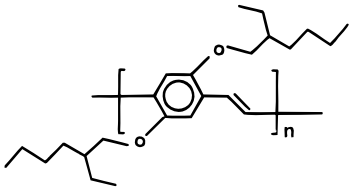

EH-PPV

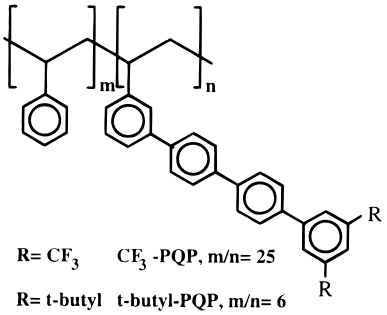

R= CF_3 CF_3 -PQP, m/n= 25

R= t-butyl t-butyl-PQP, m/n= 6

rectangular voltage pulses of variable duration and variable time period between successive pulses. The EL signal was detected with a photomultiplier. An integrated sphere was employed for measuring the quantum efficiencies.

3. Results

3.1. Monomer and Polymer Synthesis. The synthesis of poly[(2,5-bis((2-ethylhexyl)oxy)phenylene)-vinylene] has been described in ref 19.

Monomer I (3-vinyl-3‴,5‴-bis(trifluoromethyl)-1,1′:4′,1″:4″,1‴-quaterphenyl) was synthesized according to Scheme 1.

The radical copolymerization of Ib with styrene shows nearly statistical incorporation of both monomers (Scheme 2, Table 1). The polymerization rate of Ib is smaller than that of styrene. The copolymers are amorphous and soluble in toluene, chloroform, THF, cyclohexane, and methylcyclohexane. The amorphous character of the polymer is obvious from DSC and X-ray measurements.

T_g increases with higher amounts of Ib.

λ_{max} of the UV absorption of copolymers with Ia as well as with Ib is 300 nm, whereas the fluorescence differs: 369 nm with Ib and 389 nm with Ia.

3.2. Electroluminescence. $j(E)$ characteristics for single-layer diodes of CF_3-PQP and *tert*-butyl-PQP sandwiched between ITO and Ca electrodes are shown in Figure 1. It is obvious that the replacement of the *tert*-butyl groups by the strongly electron-withdrawing CF_3 groups leads to a significant enhancement of the current. With bilayer LEDs of the type ITO/TSA:PSu/CF_3-PQP/cathode the cell current under forward bias increases with decreasing workfunction of the cathode (Figure 2). If one compares the $j(E)$ characteristics obtained with a Ca cathode with either the hole current injected from ITO into a single-layer TSA:PSu diode or the electron current injected from Ca into CF_3-PQP, one

Scheme 1. Synthesis of Quaterphenyl Ib

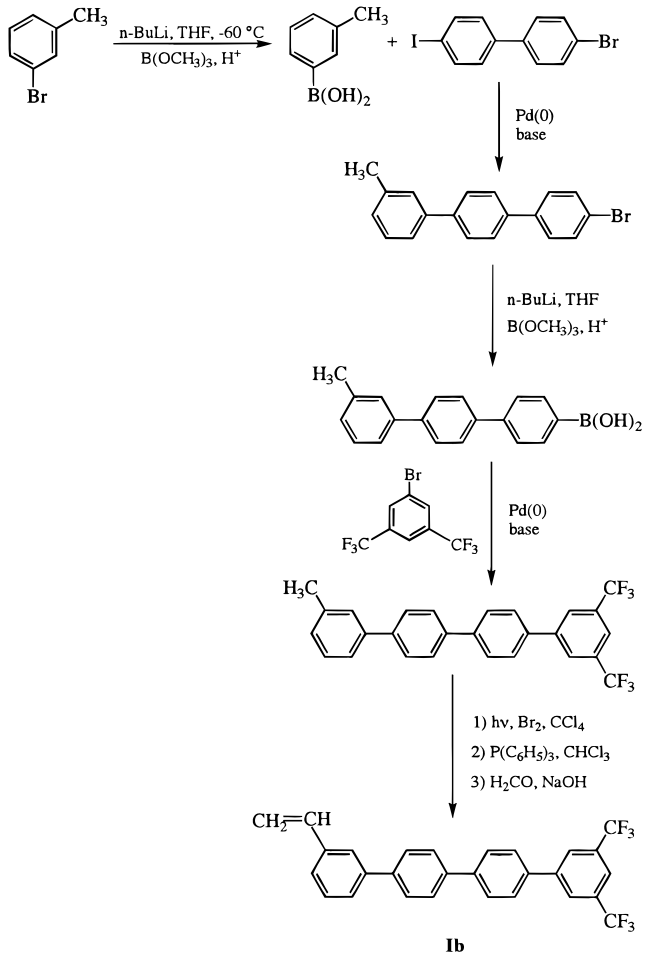

Ib

realizes that the combination of both transport materials in a bilayer LED depresses the current by several orders of magnitude depending on the applied electric field. For an ITO/TSA:PSu/*tert*-butyl-PQP/Al device, a similar reduction of the cell current as compared to the hole injection current into a single-layer TSA:PSu diode is noticed (Figure 3). With an ITO/EH-PPV:PC/*tert*-butyl-PQP/Al device the current depression is less pronounced.

When an ITO/TSA:PSu/CF_3-PQP/Ca device is addressed by rectangular voltage pulses of 500 ms duration, the electroluminescence rises abruptly after an unusually long delay time t_d and reaches saturation thereafter almost instantaneously (Figure 4). t_d decreases rapidly with decreasing waiting time t_w (Figure 5) and with increasing electric field (Figure 6). The bilayer LEDs ITO/TSA:PSu/*tert*-butyl-PQP/Mg and ITO/EH-PPV:PC/CF_3−PQP/Al show principally the same pattern of observations (Figures 7 and 8). In contrast, an ITO/EH-PPV:PC/*tert*-butyl-PQP/Al device behaves conventionally as far as the transient EL is concerned. In that case, the onset of EL correlates with the RC time (≈20 μs) constant of the circuit and saturation is attained after about 1 ms (Figure 9).

The EL spectrum is in all cases identical with the EL spectrum of a single-layer LED containing the hole-transporting component only. This indicates that all emissive recombination events take place inside the TSA:PSu and EH-PPV layers, respectively. The external quantum efficiency of the TSA:PSu/CF_3-PQP device is about 1%, more or less independent of the cathode material used.

Scheme 2. Copolymerization of Styrene with Quaterphenyl Ib to CF_3-PQP

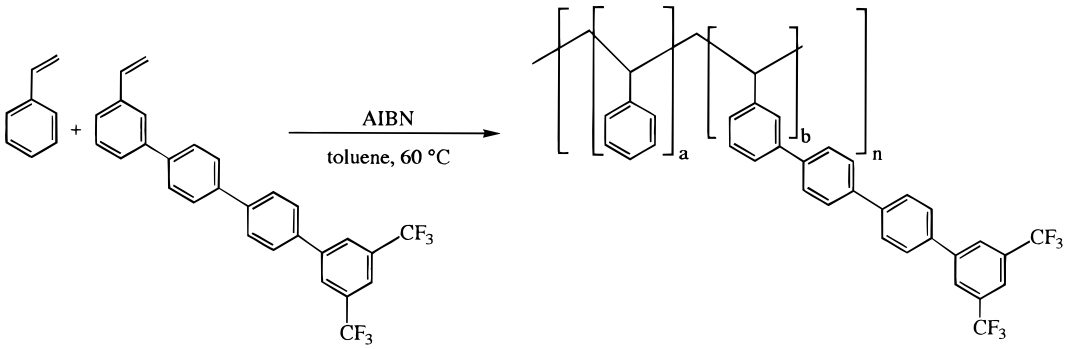

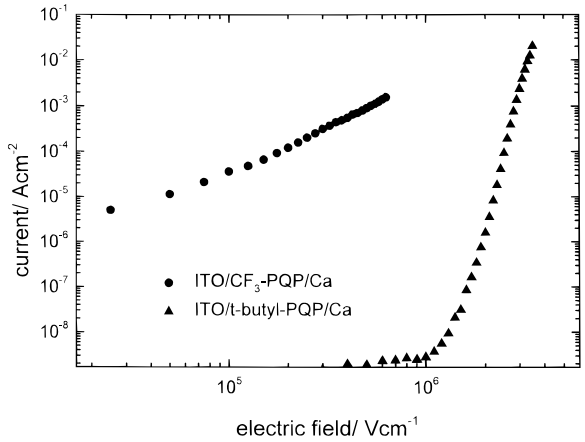

Figure 1. $j(E)$ characteristics of the electron-transporting polymers CF_3-PQP and *tert*-butyl-PQP sandwiched between ITO and Ca electrodes.

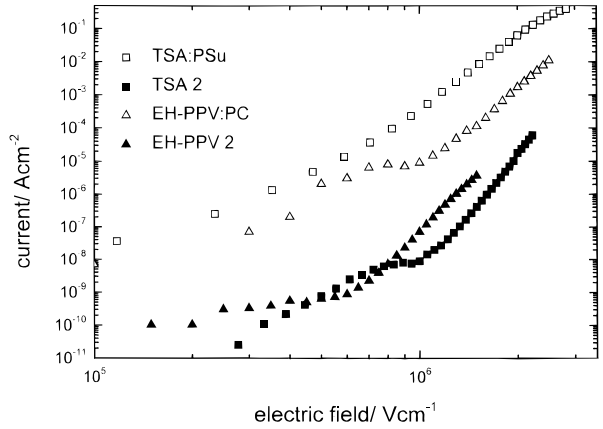

Figure 3. Comparision of the $j(E)$ characteristics of TSA:PSu/*tert*-butyl-PQP and EH-PPV:PC/*tert*-butyl-PQP devices (filled symbols) with those of TSA:PSu and EH-PPV:PC single-layer devices. In all cases Al was used as a cathode.

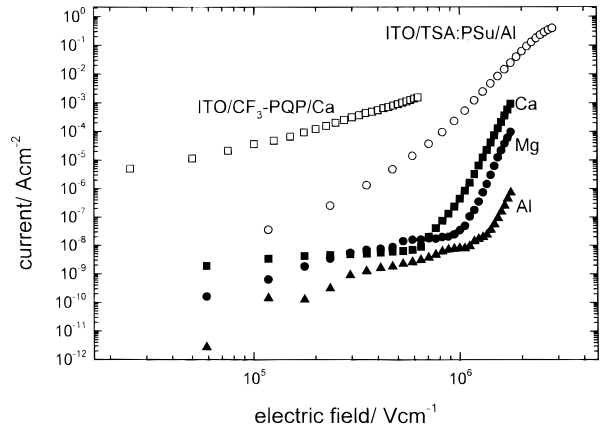

Figure 2. $j(E)$ characteristics of ITO/TSA:PSu/CF_3-PQP devices with various cathode materials (filled symbols). Data for the related single-layer devices are included for comparison (open symbols).

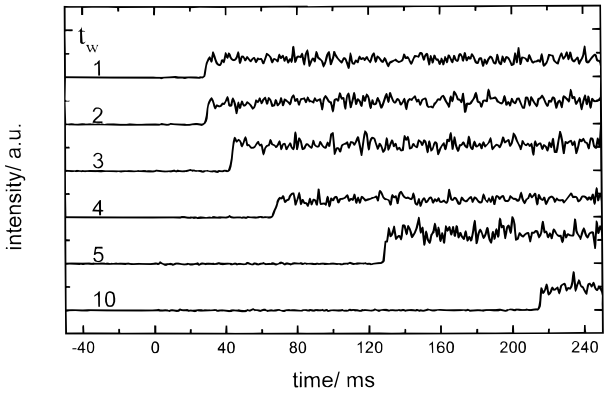

Figure 4. Transient electroluminescence of a TSA:PSu/CF_3-PQP/Ca device shown as a function of the time period (t_w) between successive voltage pulses with a constant amplitude of 22 V. Numbers indicate the time period in minutes.

4. Discussion

The information needed to understand the pattern of experimental observations is the energy level diagram of the bilayer assemblies. The diagrams shown in Figure 10 derive from the results of cyclic voltammetry (Table 2). This is the usual method of choice for measuring oxidation and reduction potentials. However, caution is in order as far as absolute values of the potentials are concerned. Cyclic voltammetry is notoriously sensitive to the experimental conditions, such as the choice of electrodes and solvents, and notably, to purity. A major problem arises when data derived from experiments in liquid solution are applied to solid state systems. In a polar solvent ions are stabilized by solvation effects due to the rearrangement of solvent dipoles in addition to some dielectric stabilization due to van der Waals interaction. In a molecular solid below the glass transition temperature where the molecules are locked in fixed positions, charge carriers can only be stabilized by van der Waals interaction between the charge and both induced and permanent dipole moments of the environment. As a result, the stabilization energy is less than that in polar liquids and depends on the electronic polarization energy of the molecules comprising the solid. Therefore cyclic voltammetry underestimates the absolute values of oxidation and reduction potentials in the solid phase. What is reliably predicted are relative changes in a homologous series in which the electronic polarizability is virtually constant. Another problem arises when either E_{ox} or E_{red}

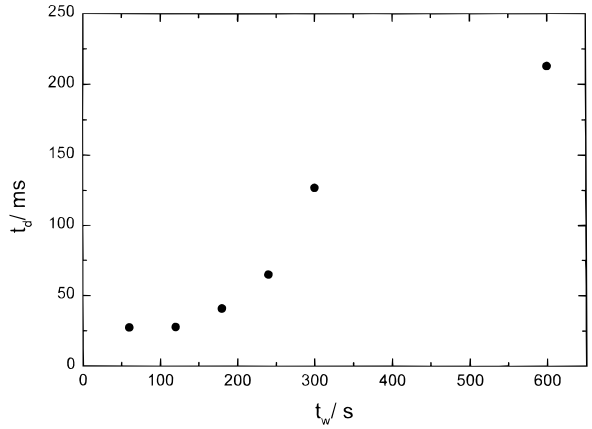

Figure 5. Dependence of the delay time t_d on the time period t_w of successive voltage pulses for a TSA:PSu/CF_3-PQP/Ca device as shown in Figure 4.

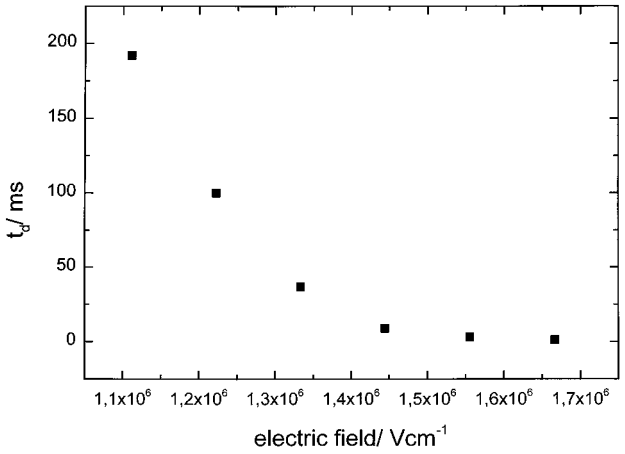

Figure 6. Field dependence of the delay time t_d of a TSA:PSu/*tert*-butyl-PQP/Mg system.

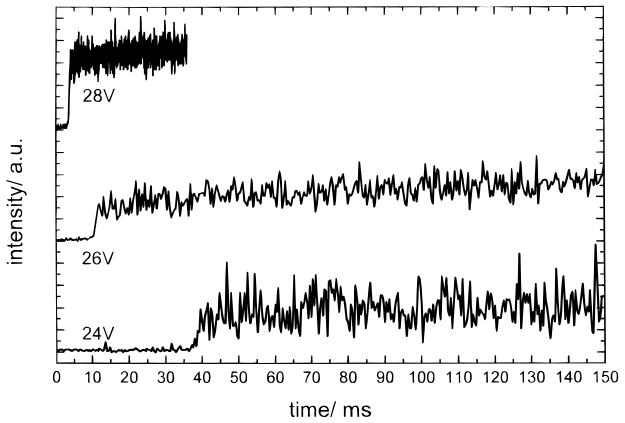

Figure 7. Transient electroluminescence of a TSA:PSu/*tert*-butyl-PQP/Mg device parametric in the amplitude of the voltage pulse.

is outside the accessible instrumental regime. In that case one often estimates the missing potential on the premise that $E_{ox} - E_{red}$ be equal to the optical $S_1 \leftarrow S_0$ 0−0 gap. This procedure ignores the Coulombic binding energy it costs to dissociate a singlet exciton into free charge carriers, i.e., a pair of Coulombically unbound radical cations and anions. Recent experiments indicate that it should be ≈0.4 eV[20,21] although values up to 0.9 eV have been reported for PPV.[22] The situation becomes even more complicated at the internal surface between the electron- and hole-transporting layers in LEDs

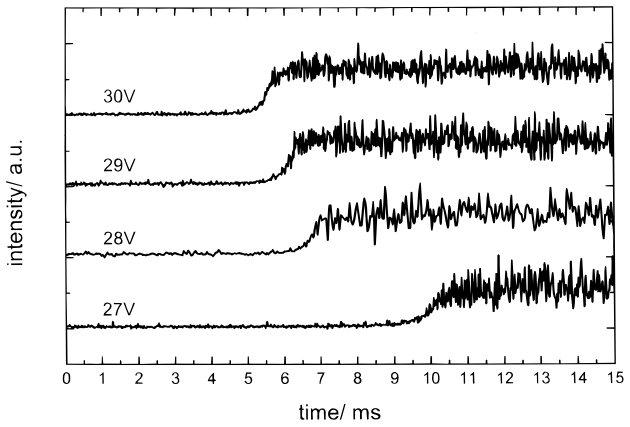

Figure 8. Transient electroluminescence of a EH-PPV:PC/CF_3-PQP/Al device as a function of the amplitude of the voltage pulse.

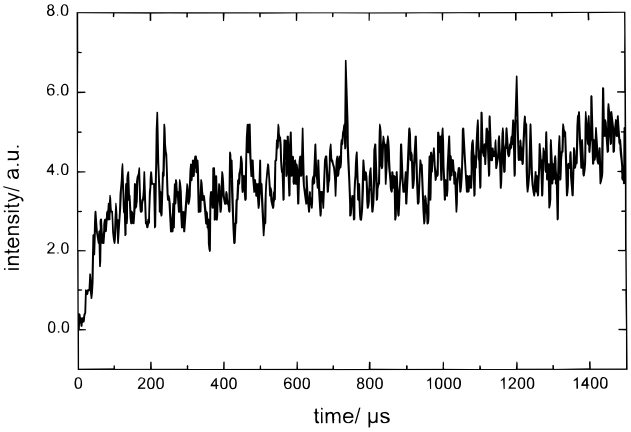

Figure 9. Transient electroluminescence of an EH-PPV:PC/*tert*-butyl-PQP/Al device upon applying a rectangular voltage pulse of 500 ms width and 30 V amplitude.

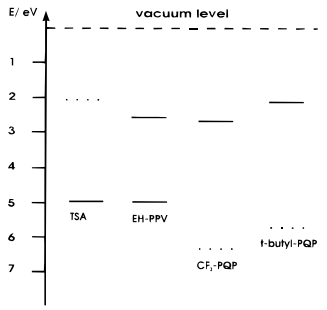

Figure 10. Energy level diagramm of the used materials. Data have been inferred from cyclic voltammetry (see Table 2). For TSA and CF_3-PQP only the oxidation potential and the reduction potential were measured, respectively. The lacking levels (dotted lines) were estimated on the basis of the optical gap.

carrying polar groups whose orientation at the interface is unknown.

The message that can be extracted from the energy level diagram of Figure 10 after considering the above cautionary remarks is that (i) the LUMO of CF_3-PQP should be between 0 and 0.3 eV above the Fermi level of a (clean) Ca electrode, (ii) the LUMO of *tert*-butyl-PQP should roughly be 0.5 eV above that of CF_3-PQP, (iii) there should be a large barrier (≈0.8 ± 0.2 eV) for electron transfer from CF_3-PQP to TSA and a barrier of roughly half that magnitude for electron transfer from CF_3-PQP to EH-PPV, while the LUMO−LUMO gap at a *tert*-butyl-PQP interface should be close to zero, and

Table 2. Electrochemical Reduction and Oxidation Potentials ($E_{1/2}$) Determined by Cyclic Voltammetry Using FOC as Reference[a]

material	E_{ox}/V	E_{red}/V
TSA	0.32	
EH-PPV	0.3	−2.31
tert-butyl-PQG		−2.81
CF_3-PQP		−2.15

[a] Oxidation potentials were measured in methylene chloride solution containing 0.1 M tetrabutylammonium hexaflurophosphate (TBAHFP) as a supporting electrolyte, the scan rate being 250 mV/s. Reduction potentials were measured in THF with TBAHFP as an electrolyte. The working electrode was a gold wire. The quasireference was an Ag wire ($E_{1/2}$(FOC) = 0.463 V). Conversion into an absolute energy, required for determining HOMO and LUMO positions, was done according to Bard and Faulkner (Bard, A. J.; Faulkner, L. R. *Electrochemical Methods-Fundamentals and Applications*; Wiley: New York, 1980; p 634) by adopting the value −4.6 eV for the standard electrode potential of the normal hydrogen electrode and the value 0.2 V for the potential of FOC vs NHE (in acetonitrile, see: Koepp, H.-M.; Wendt, H.; Strehlow, H. Z. *Electrochem.* **1960**, *64*, 483).

(iv) there should be an energy barrier in excess of 1 eV for hole transport from TSA to CF_3-PQP.

Current vs field characteristics measured with single-layer PQP diodes are in accordance with those estimates. The $j(E)$ curve for the ITO/CF_3-PQP/Ca diode follows a $j \propto E^2$ relation quite closely. This is a characteristic feature of unipolar space charge limited conduction obeying Child's law.[23,24]

$$j_{SCL} = \frac{9}{8}\epsilon\epsilon_0\mu\frac{E^2}{d} \qquad (1)$$

where ϵ is the dielectric constant, ϵ_0 is the permittivity of free space, μ is the average carrier mobility, and d is the sample thickness. It requires that one contact acts as an inexhaustible reservoir of one sort of charge carrier. Applying eq 1 to the data of Figure 1 yields an electron mobility $\mu_- = 8 \times 10^{-9}$ cm^2/(V s). Considering that only the substituents, i.e., only 13% (by weight) of CF_3-PQP, act as hopping sites for electrons and that, by and large, the mobility decreases exponentially with intersite concentration, this appears to be a realistic number, the more so because the twisted ground state conformation of the quaterphenyl unit implies some structural reorganization after charge attachment.

In view of the finite energy barrier for electron injection from Ca into *tert*-butyl-PQP the condition of having an ohmic contact is no longer fulfilled and the current is limited by injection rather than by the space charge of the transported charge carriers. This is borne out by the $j(E)$ curve. If one plotted $\ln(j/E^2)$ vs E^{-1}, appropriate for testing Fowler−Nordheim tunneling injection, one obtained a curve that approaches a straight line at high fields extending over 2 decades and yielding an injection barrier of 0.7 eV.

The energy level diagram also indicates that in a TSA:PSu/CF_3-PQP LED the passage of electrons should be impeded by an internal energy barrier $\chi_e = 0.8$ eV while the related barrier for hole transport is estimated as $\chi_h = 1.5$ eV. The corresponding values for TSA:PSu/*tert*-butyl-PQP are $\chi_e = 0.1$ eV and $\chi_h = 0.8$ eV, while those for EH-PPV/CF_3-PQP are $\chi_e = 0.3$ eV and $\chi_h = 0.8$ eV. The $j(E)$ characteristics are a reflection of the transport of majority carriers being impeded by a large energy barrier. Consider the TSA:PSu/CF_3-PQP case first, for which the injection currents into the respective single-layer devices are known (see Figure 2). The current is orders of magnitude smaller than either of the unipolar injection currents expected if the electric field, calculated for the applied voltage and the sample thickness, acted on the injecting contacts. The reason is that the formation of a charged double layer generated by the accumulating positive and negative space charge at the anodic and the cathodic side of the interface screens the electric field at the contacts. Under steady state conditions the current had to decay to zero unless recombination and some carrier leakage occurred at the interface. The rate-limiting step will, therefore, be recombination at the interface. It neutralizes some of the space charge and ensures that a finite, albeit smaller, electric field maintains at the anode. Reducing electron injection by using Mg or Al as cathode materials will cut down the number of holes that can be neutralized per unit time at the interface via recombination with electrons and, concomitantly, hole injection to replenish the internal space charge.

The unusually steep and delayed onset of EL can be understood as a direct reflection of the high interfacial energy barrier that prevents thermal barrier crossing. Note that the onset of EL in single-layer LEDs or bilayer LEDs with small energy barriers for minority carriers, realized, for instance, in an ITO/EH-PPV:PC/*tert*-butyl-PQP/Al LED (Figure 9), occurs quite smoothly and reflects charge transport into the recombination zone.[24−26] The magnitude of the delay time and the concomitant rapid increase of EL for $t > t_d$, borne out by Figure 4, cannot be identified with a time of flight signal since in random media the latter should feature a broad tail whose decay time is of order of the transit time itself provided that transport occurs under equilibrium conditions. Otherwise, the tail is even more extended, if discernible at all.[27] The alternative explanation is in terms of interfacial charging up to a value that allows electrons to tunnel into the hole-transporting layer where recombination occurs. In principle, this process is contained in the analytic treatment of bilayer LEDs by Khramtchenkov et al.[28,29] Although analytically exact, it does not, unfortunately, allow for a straightforward evaluation of the dependences of the EL intensity. For this reason a simple model shall be advanced instead, appropriate under the condition that interfacial barrier crossing rather than injection from the electrodes is the rate-limiting step.

Consider the TSA:PSu/ CF_3-PQP case depicted schematically in Figure 10. The ohmic nature of the Ca cathode will ensure that electrons accumulate at the internal interface and build up an interfacial charge density. Ignoring Coulombic effects as well as disorder-mediated level broadening, they face a triangular energy barrier that cannot be overcome thermally. However, upon arrival of holes that were injected from the ITO anode under the assistance of the electric field, a positive charge will accumulate at the opposite side of the interface. As a consequence, the barrier narrows and eventually tunneling commences. In view of the lower barrier for electrons, it will be the latter that penetrate the barrier and neutralize holes thus, generating an emissive exciton in the hole-transporting layer. If $N_{+/-}$ denotes the area densities of interfacial positive and negative charges,

$$\dot{N}_+ = \dot{N}_- = \frac{j_+}{e} - N_+k \qquad (2)$$

where j_+/e is the number of holes arriving at the

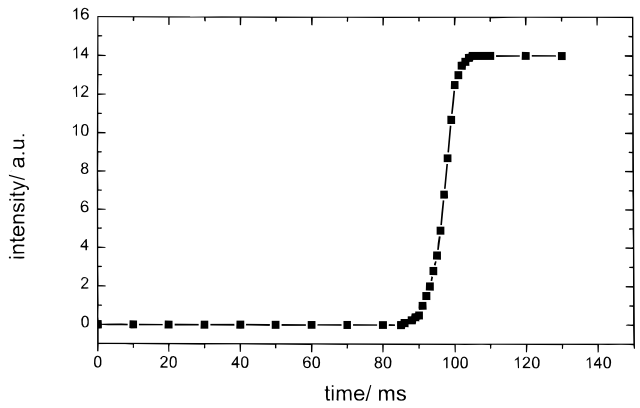

Figure 11. Calculated time dependence of the El intensity of a model system based on eq. 7 with parameters $\nu_0 = 10^{13}$ s^{-1}, $\chi_e = 1$ eV, and $j = 10^{-5}$ A cm^{-2}.

interface per unit area and time and N_+k is the loss term, due to electron tunneling. The simplest assumption for k is

$$k = \nu_0 \exp\left[-\frac{b}{E}\right] \tag{3}$$

where ν_0 is a prefactor and the second term has the form of a Fowler−Nordheim-type tunneling probability,

$$b = \frac{4\sqrt{2}m_{\text{eff}}}{3\hbar e}\chi_e^{3/2} \tag{4}$$

If one makes the usual assumption[2] that the effectvive mass is set equal to the free electron mass, $b = 7.1 \times 10^7 \chi_e^{3/2}$ (V/cm) if the barrier height χ_e is given in electron volts. The electric field E can be expressed via the interfacial charge densities,

$$E = (N_0 + N_+)/\epsilon\epsilon_0 \tag{5}$$

where N_0 is the negative charge density at the beginning of the field-driven supply of minority carriers. The EL intensity will be proportional to N_+k. In the early time domain $N_+(t) + \int_0^t (j_+/e)\,dt$, which reduces to

$$N_+(t) = (j_+/e)t \tag{6}$$

under the simplifying assumption of time independent hole injection. Combining eqs 2−6 yields

$$I_{\text{EL}} \propto N_+k = (j_+/e)\nu_0 t \exp\left[-\frac{\epsilon\epsilon_0 b\chi_e^{3/2}}{N_0 + (j_+/e)t}\right] \tag{7}$$

as long as $t < t_{\text{eq}}$, where t_{eq} is the time after which steady state conditions have been established. For $t > t_{\text{eq}}$, the condition $\dot{N}_+ = 0$ yields

$$\nu_0 t_{\text{eq}} \exp\left[-\frac{\epsilon\epsilon_0 b\chi_e^{3/2}}{N_0 + (j_+/e)t_{\text{eq}}}\right] = 1 \tag{8}$$

Onset of EL will be governed by the exponential term in eq 7. As far as the shape of the rising edge of EL is concerned, the magnitude of N_0 is unimportant. There is a critical space charge density above which efficient tunneling commences and the term $(j_+/e)t_{\text{eq}}$ in the denominator of the exponent in eq 7 indicates the amount of charge that has to be supplied via minority carrier injection. In Figure 11 the time dependence of EL calculated on the premise of the parameter choice $\nu_0 = 10^{13}$ s^{-1}, $\chi_e = 1$ eV, and $j = 10^{-5}$ A/cm^2 is shown. It is obvious that the observed steep increase of EL after a delay time of order 100 ms is recovered. The appearance of t in the exponent precludes a straightforward integration of eq 2. Bearing in mind, however, that for $t \approx t_{\text{eq}}$ the interfacial charge density changes very little, turn-over to steady behavior is close to that of a unimolecular reaction with time independent rate constant N_+k. The time profile in Figure 11 has been drawn on this premise, implying that t_d and t_{eq} are virtually identical.

The agreement between the shapes of the experimental and calculated EL(t) profiles in the case of bilayer LEDs with large internal electron barriers (the broadening of the temporal profile in the TSA:PSu/*tert*-butyl-PQP system in which the electron barrier is significantly smaller and in conjuntion the absence of the effect in the EH-PPV:PC/*tert*-butyl-PQP system in which χ_e is close to zero) indicates that, despite its simplicity, the model advanced above grasps the essential physics of the transient EL behavior of the bilayer systems studied. It accounts for the unusually sharp onset of EL, reminescent of the evolution of electrical breakdown, and for the field dependence of the delay time. Since the latter is determined by charge accumulation, it must be related to the amount of charge flowing during $0 < t < t_d$. The field dependence of t_d should therefore be determined by the condition $t_d(E)j_+(E) = \text{const}$. In experiment, t_d decreases somewhat faster than expected on the basis of the measured current. However, since the measured current is a superposition of several current contributions, this is all but surprising. It is worth noting that for the parameter set used to obtain Figure 11 the critical electric field acting at the interface where tunneling commences is 3×10^6 V/cm.

Of particular interest is the decrease of t_d with decreasing time period (t_w) between successive voltage pulses. Since the delay time is governed by the condition $N_0 + (j_+/e)t_d = \text{const}$, a decrease of t_d is a signature of a higher remnant charge density. Measurement of t_d as a function of T provides, therefore, insight into the depletion of the interfacial double layer after switching of the external voltage. In conventional bilayer systems in which the internal energy barrier for electrons is small enough to be overcome thermally, the decay of the interfacial charge is an ordinary first-order rate process, completed within a time scale of typically 10 μs to 10 ms. If barrier crossing is a tunneling process, decay of the interfacial charge at the end of the voltage pulse slows down dramatically if the charge density falls below the critical limit. In that case the bilayer can persist for minutes. The ultimate depletion is likely to be governed by inefficient direct transition between the radical cation in the hole-transporting zone and the radical anion in the electron-transporting zone. To derive more quantitative information concerning interfacial charge depletion would require a systematic study of the dependence of t_d on t_w.

Equation 7 predicts that the transient EL behavior is sensitive to the magnitude of χ_e. However, the structure of eq 7 implies that this dependence is a very weak one. In systems with smaller χ_e additional interfacial charge accumulation, governed by the product j_+t_d, will be completed at shorter time. In practice, this effect is likely to be masked by the inevitable variation in the current density upon changing the materials and, concomitantly, the injection barriers. This explains why the bilayer systems ITO/TSA:PSu/

tert-butyl-PQP/Mg and ITO/EH-PPV:PC/CF_3-PQP/Al behave similarly to the ITO/TSA:PSu/CF_3-PQP/Ca system. A qualitative change of the device behavior is not expected until χ_e falls below the critical value at which thermal barrier crossing becomes competitive with barrier crossing by tunneling, as realized in the EH-PPV:PC/*tert*-butyl-PQP case. Neither does it matter which sort of carrier is the majority/minority carrier as long as it is guaranteed that both are blocked at the internal interface.

5. Concluding Remarks

One of the essential results of this study is the verification that substituted quarterphenyl attached to an aliphatic polymeric chain can profitably be used as electron-transporting material in bilayer LEDs. Its advantages include its resistence against crystallization and the magnitude of reduction and oxidation potentials. A low-lying LUMO guarantees improved electron injection properties, while the low-lying HOMO ensures efficient hole-blocking properties even if combined with hole-transporting materials that are not optimized as far their oxidation potential is concerned.

In the present paper the physical aspects of the operation of bilayer LEDs prepared with PQP as the electron transport layer have been emphasized. It has been demonstrated that in combination with conventional hole-transporting materials the current flow through the device is controlled by internal barrier crossing and, concomitantly, carrier recombination rather than by carrier leakage toward the electrodes. By this token one crucial condition for efficient device operation is met. Another result of the present study is the successful demonstration of sort of a switching behavior concerning transient EL behavior upon addressing the device by voltage pulses. It is the consequence of tunneling processes being the rate-limiting step and can establish the basis for designing LEDs with short switching times.

Acknowledgment. We are indepted to Dr. K. Kelnhofer and Prof. J. Daub for performing cyclic voltammetry measurements. Stimulating discussion with D. Khramtchenkov concerning the theory of LED operation is gratefully acknowledged. This work was supported by the Bundesministerium für Bildung, Wissenschaft, Forschung, und Technologie (BMBF).

References and Notes

(1) Albrecht, U.; Bässler, H. *Chem. Phys.* **1995**, *199*, 207.
(2) Parker, I. D. *J. Appl. Phys.* **1994**, *75*, 1656.
(3) Vestweber, H.; Pommerehne, J.; Sander, R.; Mahrt, R. F.; Greiner, A.; Heitz, W.; Bässler, H. *Synth. Met.* **1995**, *68*, 263.
(4) Brown, A. R.; Burroughes, J. H.; Greenham, N. C.; Friend, R. H.; Bradley, D. D. C.; Burn, P. L.; Kraft, A.; Holmes, A. B. *Appl. Phys. Lett.* **1992**, *61*, 2703.
(5) Thang, C.; Hoeger, S.; Pakbaz, K.; Wudl, F.; Heeger, A. J. *J. Electron. Mater.* **1994**, *23*, 453.
(6) Baigent, D. R.; Greenham, N. C.; Grüner, J.; Marks, R. N.; Friend, R. H.; Moratti, S. C.; Holmes, A. B. *Synth. Met.* **1994**, *64*, 3.
(7) Pommerehne, J.; Vestweber, H.; Guss, W.; Mahrt, R. F.; Bässler, H.; Porsch, M.; Daub, J. *Adv. Mater.* **1995**, *7*, 551.
(8) Hosokawa, C.; Higashi, H.; Nakamura H.; Kusumoto, T. *Appl. Phys. Lett.* **1995**, *67*, 3853.
(9) Adachi, C.; Tokito, S.; Saito, S. *Jpn. J. Appl. Phys.* **1988**, *27*, L269.
(10) Tang, C. W.; vanSlyke, S. A. *Appl. Phys. Lett.* **1987**, *51*, 913.
(11) Thelekkat, M.; Früh, R.; Pösch, P.; Ring, J.; Schmidt, H. W. *Polym. Prepr. (Am. Chem. Soc., Div. Polym. Chem.).*
(12) Pei, Q.; Young, Y. *Adv. Mater.* **1995**, *7*, 559.
(13) Adachi, C.; Tsutsui, T.; Saito, S. *Appl. Phys. Lett.* **1989**, *55*, 1489.
(14) Bradley, D. D. C. *Synth. Met.* **1993**, *54*, 401.
(15) Salbeck, J. *Ber. Bunsen-Ges. Phys. Chem.* **1996**, *100*, 1667.
(16) Wirth, H. O.; Königstein, O.; Kern, W. *Liebigs Ann. Chem.* **1960**, *84*, 643.
(17) Deng, G.; James, T.; Shinkai, S. *J. Am. Chem. Soc.* **1994**, *116*, 4567.
(18) Sander, R.; Stümpflen,V.; Wendorff, J. H.; Greiner, A. *Macromolecules* **1996**, *29*, 7705.
(19) Koch, F.; Heitz, W. *Macromol. Chem. Phys.* **1997**, *198*, 1531.
(20) Deussen, M.; Scheidler, M.; Bässler, H. *Synth. Met.* **1995**, *73*, 123.
(21) Barth, S.; Deussen, M.; Bässler, H. *Phil. Trans. R. Soc. London A* **1997**, *355*, 749.
(22) Chandross, M.; Mazumdar, S.; Jeglinski, S.; Wei, X.; Vardeny, Z.; Kwock, E. W.; Miller, T. M. *Phys. Rev. B* **1992**, *50*, 14702.
(23) Blom, P. W. M.; de Jong, M. J. M.; Vleggar, J. J. M. *Appl. Phys. Lett.* **1996**, *68*, 3308.
(24) Tak, Y. H.; Vestweber, H.; Bässler, H.; Bleyer, A.; Stockmann, R.; Hörhold, H. H. *Chem. Phys.* **1996**, *212*, 471.
(25) Hosokawa, C.; Tokailin, H.; Higashi, H.; Kusumoto, T. *Appl. Phys. Lett.* **1992**, *60*, 1220.
(26) Pommerehne, J.; Vestweber, H.; Tak, Y. H.; Bässler, H. *Synth. Met.* **1996**, *76*, 67.
(27) Bässler, H. *Phys. Stat. Sol. B* **1993**, *175*, 15.
(28) Khramtchenkov, D. V.; Bässler, H.; Arkhipov, V. I. *J. Appl. Phys.* **1996**, *79*, 9283.
(29) Khramtchenkov, D. V.; Arkhipov, V. I.; Bässler, H. *J. Appl. Phys.* **1997**, *81*, 6954.

MA9709056